

Contrasting Trivalent Lanthanide and Actinide Complexation by Polyoxometalates via Solution-State NMR

Christopher A. Colla, Ian Colliard, April M. Sawvel, May Nyman, Harris E. Mason, and Gauthier J.-P. Deblonde*



Cite This: *Inorg. Chem.* 2023, 62, 6242–6254



Read Online

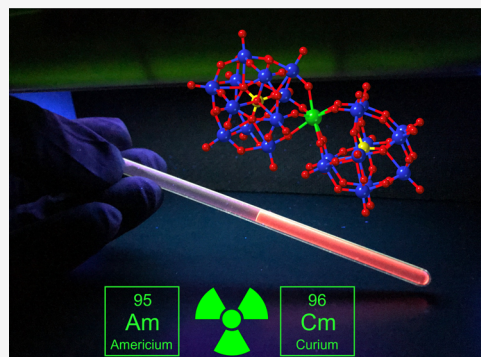
ACCESS |

Metrics & More

Article Recommendations

Supporting Information

ABSTRACT: Deciphering the solution chemistry and speciation of actinides is inherently difficult due to radioactivity, rarity, and cost constraints, especially for transplutonium elements. In this context, the development of new chelating platforms for actinides and associated spectroscopic techniques is particularly important. In this study, we investigate a relatively overlooked class of chelators for actinide binding, namely, polyoxometalates (POMs). We provide the first NMR measurements on americium–POM and curium–POM complexes, using one-dimensional (1D) ^{31}P NMR, variable-temperature NMR, and spin-lattice relaxation time (T_1) experiments. The proposed POM–NMR approach allows for the study of trivalent f-elements even when only microgram amounts are available and in phosphate-containing solutions where f-elements are typically insoluble. The solution-state speciation of trivalent americium, curium, plus multiple lanthanide ions (La^{3+} , Nd^{3+} , Sm^{3+} , Eu^{3+} , Yb^{3+} , and Lu^{3+}), in the presence of the model POM ligand $\text{PW}_{11}\text{O}_{39}^{7-}$ was elucidated and revealed the concurrent formation of two stable complexes, $[\text{M}^{\text{III}}(\text{PW}_{11}\text{O}_{39})(\text{H}_2\text{O})_x]^{4-}$ and $[\text{M}^{\text{III}}(\text{PW}_{11}\text{O}_{39})_2]^{11-}$. Interconversion reaction constants, reaction enthalpies, and reaction entropies were derived from the NMR data. The NMR results also provide experimental evidence of the weakly paramagnetic nature of the Am^{3+} and Cm^{3+} ions in solution. Furthermore, the study reveals a previously unnoticed periodicity break along the f-element series with the reversal of T_1 relaxation times of the 1:1 and 1:2 complexes and the preferential formation of the long T_1 species for the early lanthanides versus the short T_1 species for the late lanthanides, americium, and curium. Given the broad variety of POM ligands that exist, with many of them containing NMR-active nuclei, the combined POM–NMR approach reported here opens a new avenue to investigate difficult-to-study elements such as heavy actinides and other radionuclides.



INTRODUCTION

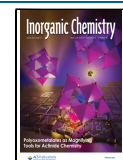
Polyoxometalates (POMs), metal-oxo clusters of the group five and six metals (i.e., tungstates, molybdates, vanadates, niobates, and tantalates), present rich and diverse aqueous speciation under ambient conditions that is controlled predominantly by pH and counterions.^{1–3} The diversity in geometric structure, electronic structure, as well as primary and substituent metals within the POM family is vast, and POMs offer an inorganic alternative to organic ligands typically studied for metal binding. POMs range in molecular weight and size from the relatively small Lindqvist ($\text{M}_6\text{O}_{19}^{n-}$) and Keggin ($\text{XM}_{12}\text{O}_{40}^{n-}$, where X is a heteroatom and M is a group V or VI element) ions to large cages and wheel-like structures⁴ (e.g., Mo_{100} , Mo_{154} , Mo_{200} , and Mo_{368} wheels).^{5–8} Heteroatoms including P, B, Ge, Si, Se, As, Sb, Bi,^{9–12} and POMs can form mixed species^{13–16} (e.g., tungstate–molybdate, niobate–tantalate, tungstate–niobate, niobate–titannate, etc.). Finally, open-shell transition-metal substitution¹⁷ and lanthanide substitution¹⁸ provide nearly limitless opportunity for tailoring composition and structure in POM ligands. Studied applications relying on POMs include catalytic reactions,^{19–21}

luminescent or electrochemical sensors,²² medicine,^{23,24} electronics,²⁵ chemical warfare neutralizers,^{26,27} novel memory devices,²⁸ qubits,²⁹ molecular magnets,³⁰ and model compounds for reactions that occur at mineral–water interfaces.^{31,32}

In detail, POMs such as polyoxotungstates are anionic species with multiple basic oxygens and represent potential chelators for lanthanide and actinide cations. Exploiting POM's basic oxygens and open coordination sites to complex actinides (and lanthanide surrogates) is of particular interest for novel chemical immobilization and/or separation methods in the frame of the nuclear fuel cycle and nuclear waste management. From a fundamental point of view, studying actinide–POM complexes could also unravel speciation and structure trends

Received: November 14, 2022

Published: December 29, 2022



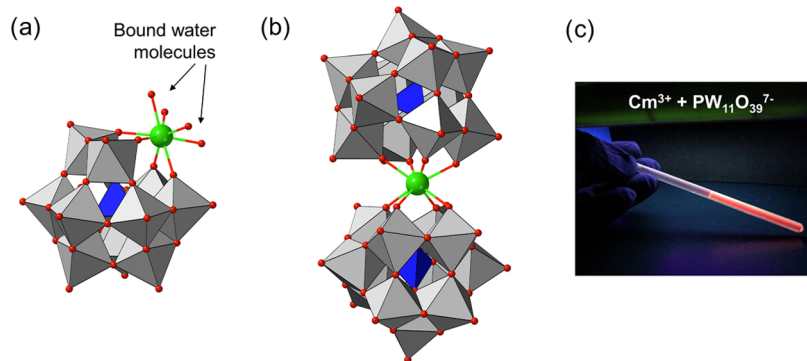


Figure 1. Polyhedral representations of the cluster species studied in this work. (a) Depiction of the 1:1 Ln^{3+} :POM or An^{3+} :POM complex. (b) Structure of the 1:2 Ln^{3+} :POM or An^{3+} :POM complex. Gray octahedra contain W^{6+} , blue tetrahedra contain P^{5+} , the small red spheres are oxygen anions, and the large green spheres represent Ln^{3+} or An^{3+} cations. Notice in the 1:1 complex that the geminal oxygens are coordinated water molecules. Ln = lanthanide. An = actinide. POM = $\text{PW}_{11}\text{O}_{39}^{7-}$. (c) Photograph of the curium–POM sample used for NMR experiments. Under UV light, the sample exhibits intense pink-orange fluorescence once the POM and curium are mixed together (due to fluorescence sensitization of Cm^{3+} via the POM ligand and subsequent intramolecular energy transfer).³⁹ This confirmed the effective complexation of the Cm^{3+} ions by the POM ligand prior to NMR measurements. The sample is transparent and is not luminescent under normal light. Additional photographs are shown in Figure S1.

that have not been observed before since POMs represent a versatile suite of molecules with properties that readily differ from those of traditional organic chelators or small inorganic ligands. Previous studies have focused on lanthanide–POM complexes in solution and solid state,^{33–35} but the use of POMs in actinide sciences has remained largely unexplored. In particular, the interactions between lacunary POM chelators (“lacun” meaning open coordination sites for complexation) and the analogous trivalent actinides (i.e., Ac^{3+} , Pu^{3+} , Am^{3+} , Cm^{3+} , Bk^{3+} , etc.) are still mostly unknown, limiting our ability to understand periodic trends within f-element–POM families of complexes. Multiple studies have reported on POM chemistry with thorium, uranium, and neptunium, as summarized in a recent review,³⁶ but minimal information is available concerning POM complexes with the other actinides (e.g., Ac, Pu, Am, Cm, Bk, etc.), mainly due to their radiotoxicity as well as scarcity and cost of their research isotopes. For example, beyond neptunium, only a handful of POM–actinide complexes have been structurally characterized to date. Notably, until very recently, only three single-crystal X-ray diffraction (XRD) structures for transneptunium–POM compounds were known, with one study published in 2009 by Copper et al.³⁷ on the complex formed between PuO_2^{2+} and $\text{GeW}_9\text{O}_{34}^{10-}$, and another study by Sokolova et al.,³⁸ also in 2009, on the complexes of Pu^{4+} and Am^{4+} with $\text{P}_2\text{W}_{17}\text{O}_{61}^{10-}$. In 2022, our group doubled the number of structurally characterized transneptunium–POM compounds by reporting³⁹ the first three single-crystal XRD structures of curium–POM complexes, namely, $\text{Cm}^{\text{III}}(\alpha\text{-PW}_{11}\text{O}_{39})_2^{11-}$, $\text{Cm}^{\text{III}}(\beta\text{-PW}_{11}\text{O}_{39})_2^{11-}$, and $\text{Cm}^{\text{III}}(\text{BW}_{11}\text{O}_{39})_2^{15-}$. Information on transneptunium–POM complexes in solution has been limited to a handful of pioneering studies on $\text{Pu}^{4+/3+}$, $\text{Am}^{4+/3+}$, Cm^{3+} , $\text{Bk}^{4+/3+}$ in the presence $\text{P}_5\text{W}_{30}\text{O}_{110}^{15-}$, $\text{PW}_{11}\text{O}_{39}^{7-}$, $\text{SiW}_{11}\text{O}_{39}^{8-}$, and $\text{P}_2\text{W}_{17}\text{O}_{61}^{10-}$, using cyclic voltammetry,^{40,41} fluorescence spectroscopy, or tracer-level experiments using liquid–liquid extraction.^{42–45} These prior studies aimed at determining the redox potentials of the actinide–POM complexes or at determining their formation constants.

To the best of our knowledge, nuclear magnetic resonance (NMR) spectroscopy has never been used to investigate the complexation of POMs to actinides other than Th and U.

Being able to probe heavy actinide–POM complexes by solution-state NMR could reveal chemical information and complexation properties that cannot be observed by other techniques. For example, NMR spectroscopy probes specific elemental sites on a molecule and can inform the speciation as well as magnetic behavior of the complexes in solution. NMR is also a nondestructive analysis, a prerequisite for precious samples like heavy actinides, and is compatible with most f-element cations, including those that do not exhibit the properties typically used to study actinide compounds, such as luminescence or spectrophotometric absorbance. Moreover, NMR spectroscopy appears ideally suited to study the POM–actinide complexes since many of the heteroatoms that can be inserted in POMs are NMR-active nuclei, including ^{31}P , $^{10/11}\text{B}$, ^{75}As , ^{77}Se , and ^{29}Si . For instance, the tetrahedral PO_4^{3-} site embedded in phosphotungstate Keggin anions has been shown to give sharp signals in ^{31}P NMR spectra⁴⁶ and can be used to decipher their complexes’ speciation in solution. In addition, variable-temperature NMR (VT-NMR) experiments can yield solution thermodynamics and kinetics information.⁴⁷ NMR spectroscopy has previously been used to determine the rates of chemical and isotopic exchange reactions in a range of uncomplexed POMs,^{48–50} providing valuable information on assembly-disassembly processes. Finally, spin-lattice relaxation times can be measured to determine molecular size as a function of temperature and pressure,^{51,52} adding an extra analytical dimension to probe metal/ligand complexes.

Despite the rich chemical insight that NMR can offer, use of NMR spectroscopy with actinides, and particularly the transneptunium or transplutonium elements, is hampered by the limited availability of NMR laboratories with the ability to handle α emitters and long-lived radionuclides, as well as the cost and low availability of the actinide research isotopes.^{53,54} A few recent solution-state studies have been performed using ^1H , ^{13}C , and/or ^{31}P NMR with actinium⁵⁵ or americium^{55–59} complexes, exploiting organic chelators, but those experiments were limited to one-dimensional (1D) NMR at room temperature. In rare cases, two-dimensional (2D) $^1\text{H}/^{13}\text{C}$ or $^1\text{H}/^{15}\text{N}$ NMR data have been reported on americium complexes with organic ligands.^{60–62} Pioneering magnetic susceptibility measurements have also been reported for

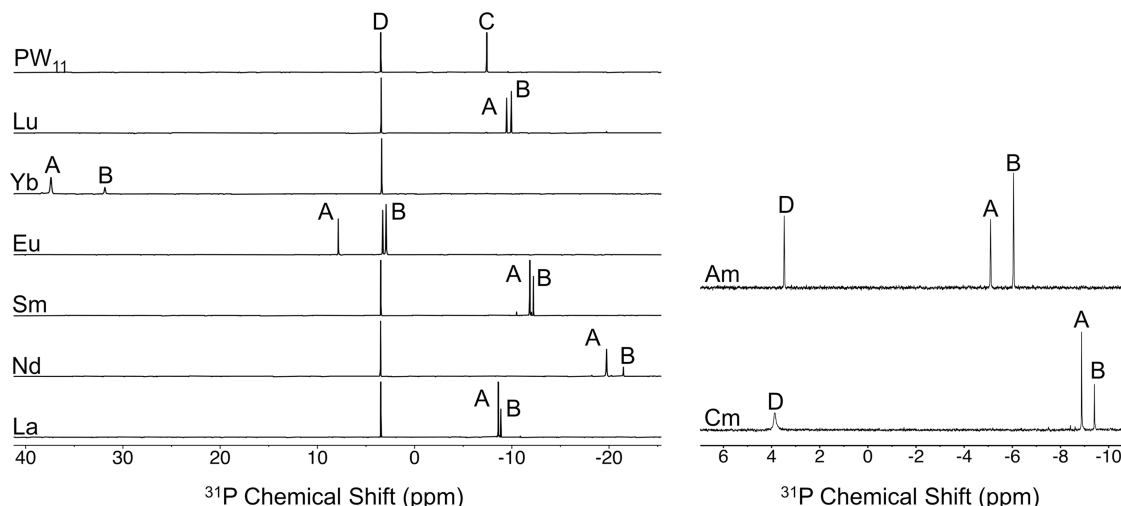


Figure 2. ^{31}P NMR spectra of Ln^- - and An^- -POM solutions studied in this work. (Left) Spectra of $\text{Ln}-\text{PW}_{11}$ samples ($\text{Ln} = \text{La}^{3+}$, Nd^{3+} , Sm^{3+} , Eu^{3+} , Yb^{3+} , or Lu^{3+}). (Right) Spectra of Am^{3+} - and Cm^{3+} - PW_{11} samples. All spectra contain two distinct NMR signals representing two separate POM species in solution. The peaks labeled A and B are assigned to the 1:1 and 1:2 metal–POM complexes, respectively. The peak labeled D is assigned to unbound phosphate ions from the buffer solution. The peak labeled C is the unchelated POM. The numerical values for the chemical shifts of the 1:1 and 1:2 metal–POM complexes are summarized in Table S1, along with their relaxometry properties (Table S2). pH = 4.5 (Buffer: 0.1 M $\text{NaCH}_3\text{COO} + 2$ mM Na_2HPO_4).

solutions of actinides in inorganic acids or actinide–organic ligand complexes.^{63–66} Rare attempts to collect ^1H and/or ^{31}P NMR data on curium or californium complexes with organic ligands have been reported to have failed due to the lack of signal attributable to the actinide species.^{55,60}

In the present work, we leverage NMR spectroscopy techniques combined with POMs to probe and contrast the solution-state behavior of trivalent lanthanides and actinides (Am^{3+} and Cm^{3+}) in solution. We study the complexation of lanthanide and actinide ions with a model polyoxotungstate ligand, namely, the mono-lacunary Keggin anion $\text{PW}_{11}\text{O}_{39}^{7-}$, via ^{31}P solution-state NMR, variable-temperature NMR, and relaxometry. The NMR experiments yield the identification of two water-soluble complexes that coexist in solution, namely, $[\text{M}^{\text{III}}(\text{PW}_{11}\text{O}_{39})(\text{H}_2\text{O})_x]^{4-}$ and $[\text{M}^{\text{III}}(\text{PW}_{11}\text{O}_{39})_2]^{11-}$, with $\text{M} = \text{Cm}^{3+}$, Am^{3+} , Lu^{3+} , Yb^{3+} , Eu^{3+} , Sm^{3+} , Nd^{3+} , or La^{3+} . The equilibrium between the two complexes was studied as a function of temperature, and the reaction enthalpies, entropies, and free energies were determined. We present the first measurements of the nuclear spin-lattice relaxation time (T_1) for transplutonium complexes and provide comparative results with multiple lanthanide–POM species. The results reveal a reversal of T_1 times of the two POM complexes as the central cation becomes heavier, representing a previously unnoticed periodicity break within the f-element series. It is our hope that this combined POM–NMR approach will open the door to the broader use of, thus far, relatively overlooked chelating agents and spectroscopic handles that can facilitate the study of actinides and advance our understanding of rare but important elements at the frontier of the periodic table.

RESULTS AND DISCUSSION

Coordination of Ln^{3+} and An^{3+} Ions by POM Ligands.

Among the variety of POMs that exist, we have selected the water-soluble phosphotungstate anion $\text{PW}_{11}\text{O}_{39}^{7-}$ for our actinide complexation study. The $\text{PW}_{11}\text{O}_{39}^{7-}$ ion is a lacunary POM and is derived from removal of a $\text{W}=\text{O}^{4+}$ moiety from the parent $\text{PW}_{12}\text{O}_{40}^{3-}$ structure. The two complexes that form

in solution and that are identified in this study are shown in Figure 1; i.e., actinide/POM species with 1:1 and 1:2 stoichiometries. The $\text{PW}_{11}\text{O}_{39}^{7-}$ ion spontaneously forms¹ upon dissolution of its precursor (the $\text{Na}_9\text{PW}_9\text{O}_{39} \cdot n\text{H}_2\text{O}$ salt;⁶⁷ see the Materials and Methods Section) in water at pH < 7. The Keggin-type $\text{PW}_{11}\text{O}_{39}^{7-}$ can have three rotational isomers, namely, α , β , and γ , which only differ by the arrangement of a subset of their WO_4^{2-} polyhedrons.⁶⁸ However, only the α isomer is expected to form in solution since it is the most stable Keggin structure.^{69,70} From a chelation perspective, the $\text{PW}_{11}\text{O}_{39}^{7-}$ ion can be viewed as a tetradentate and fully inorganic ligand (made of a PO_4^{3-} ion encapsulated by 11 tungstate octahedra) that binds metal ions through the four oxygen atoms exposed by the removal of a $\text{W}=\text{O}^{4+}$ moiety (relative to the parent $\text{PW}_{12}\text{O}_{40}^{3-}$ structure). Since lanthanide and actinide cations exhibit high coordination numbers⁷¹ in solution, typically 8 to 10, two $\text{PW}_{11}\text{O}_{39}^{7-}$ ions can satisfy the coordination environment of the f-element, or one $\text{PW}_{11}\text{O}_{39}^{7-}$ ion plus multiple solvent molecules (in the present case, water). Not surprisingly, the 1:2 complex is more readily isolated in the solid state, and our team recently crystallized 1:2 complexes of $\text{PW}_{11}\text{O}_{39}^{7-}$ with Am^{3+} , Cm^{3+} , and Ln^{3+} ions,³⁹ but the 1:1 complexes have remained elusive. As detailed hereafter, the ^{31}P NMR, VT-NMR, and relaxometry measurements demonstrate that, under the studied conditions, the 1:1 and 1:2 complexes coexist in solution, which affords an opportunity to study their equilibrium and identify periodic trends among these f-element complexes.

Solution-State ^{31}P NMR of Ln -POM and An -POM Complexes. The ^{31}P NMR spectra of solutions containing 2 equiv of $\text{PW}_{11}\text{O}_{39}^{7-}$ and 1 equiv of Am^{3+} or Cm^{3+} are shown in Figure 2. Similar experiments were performed with multiple lanthanide ions (La^{3+} , Nd^{3+} , Sm^{3+} , Eu^{3+} , Yb^{3+} , and Lu^{3+}) for comparison and to benchmark the behavior of the actinide–POM complexes. The encapsulated PO_4^{3-} ion inside the $\text{PW}_{11}\text{O}_{39}^{7-}$ cluster (Figure 1) provides an excellent spectroscopic handle, enabling the use of minute quantities of the central metal ion, which is particularly advantageous for toxic,

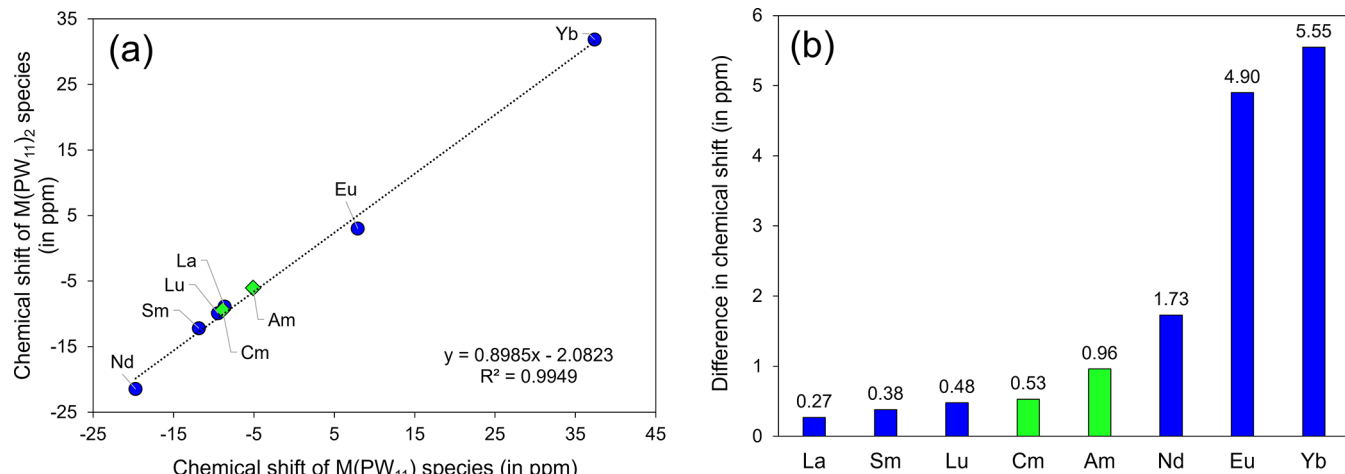


Figure 3. (a) Observed correlation between the solution-state ^{31}P NMR chemical shift of the 1:1 and 1:2 complexes formed between the trivalent lanthanide (La, Nd, Sm, Yb, and Lu) or actinide (Am and Cm) ions and the POM ligand ($\text{PW}_{11}\text{O}_{39}^{7-}$). (b) Difference in the chemical shifts of the two complexes, as a function of the central cation.

rare, and expensive elements like americium and curium. It should be noted that trivalent actinides and lanthanides are insoluble in the presence of plain phosphate ions ($\text{pK}_s \approx 25$),⁷² which prevents the direct study of their phosphate complexes at concentration levels compatible with NMR techniques. Conversely, actinide and lanthanide ions are highly soluble in the presence of $\text{PW}_{11}\text{O}_{39}^{7-}$, allowing the use of ^{31}P NMR. To minimize exposure to radiation and comply with the isotope availability, we optimized the NMR acquisition parameters, sample volumes, and sample concentrations, to perform the experiments with only $\sim 70\ \mu\text{g}$ of the actinide (i.e., $^{243}\text{Am}^{3+}$ or $^{248/246}\text{Cm}^{3+}$) per sample. The actinide samples were reused in subsequent experiments since NMR is a nondestructive technique. Experiments were performed at pH 4.5, which is compatible with the aqueous speciation of trivalent f-element ions and is within the predominance range of the $\text{PW}_{11}\text{O}_{39}^{7-}$ structure.^{1,35} Sodium phosphate was present in the buffer to serve as an internal chemical shift reference and to monitor solution pH and stability. In a recent study³⁹ performed at a slightly higher pH (5.5), spectroscopic results based on Cm^{3+} - PW_{11} fluorescence spectroscopy and UV-visible spectrophotometric absorbance measurements on Am^{3+} - PW_{11} samples suggested that the 1:1 and 1:2 complexes were present in solution, which is in line with the NMR results obtained in the present study.

Figure 2 shows the ^{31}P NMR spectra at 25 °C for all metal/POM systems studied here. In the presence of the lanthanide or actinide, three significant ^{31}P NMR signals are observed. The peak that consistently appears at +3.4 ppm (peak D in Figure 2) is assigned to unchelated phosphate ions present in the buffer. This assignment is confirmed by control experiments conducted with the buffer without POM nor the f-element (Figure S2). Solutions of the POM precursor (i.e., $\text{Na}_9\text{PW}_9\text{O}_{39} \cdot n\text{H}_2\text{O}$) dissolved in the same buffer but without lanthanide or actinide ions yield a second signal at -7.4 ppm (Peak C in Figures 2 and S2) that we assign to the unbound Keggin ion under the solution conditions selected for the present study. In addition, the spectra of Ln^{3+} -POM and An^{3+} -POM solutions show two new signals that vary both in position and in separation depending on the nature of the An^{3+} or Ln^{3+} ion (peaks A and B in Figure 2). Some of the lanthanide/POM samples also initially exhibited small addi-

tional NMR signals corresponding to transient minor constituents, which were eliminated by heating the solution or with solution aging (Figure S3). At equilibrium, the persistent observation of both peaks A and B across all chelated POM solutions suggests that two stable chelated species coexist under the solution conditions studied here. The presence of multiple f-element-POM species in solution is consistent with ^{31}P NMR spectra previously reported by Zang and co-workers³⁵ for aqueous samples of Eu^{3+} - $\text{PW}_{11}\text{O}_{39}^{7-}$ measured under different conditions ($\sim 120\times$ higher metal quantity, higher buffer concentration, different counterion, and higher complex concentration). Furthermore, the dynamic behavior of peaks A and B (Figure 2) suggests that these two species are in equilibrium with one another. We assign the least shielded peak (labeled A) as the 1:1 complex ($[\text{M}^{3+}(\text{PW}_{11}\text{O}_{39})(\text{H}_2\text{O})_x]^{4-}$) and the most shielded peak (labeled B) as the 1:2 species ($[\text{M}^{3+}(\text{PW}_{11}\text{O}_{39})_2]^{11-}$).

Depending on the lanthanide, the chemical shifts of the POM complexes are either upfield or downfield of the free phosphate ion signal at 3.4 ppm. The ^{31}P NMR signals corresponding to chelated POM species in paramagnetic solutions (Nd^{3+} , Eu^{3+} , Yb^{3+}) are shifted by tens of ppm compared to the corresponding Ln^{3+} -POM complexes in diamagnetic solutions (Figure 2). The paramagnetic lanthanides studied here result in significant paramagnetic chemical shifts, with the Yb^{3+} -POM complexes having the largest shifts. Paramagnetic chemical shifts in NMR spectra have been discussed in numerous prior studies but are worth noting here considering our choice of ligand and central cations. The paramagnetic chemical shifts observed here are likely a combination of both the pseudo-contact shift and the Fermi-contact shift.⁷³ The Fermi-contact shift is generally thought to be negligible for lanthanides that are four bonds away from the NMR nucleus.⁷⁴ In our case, the ^{31}P nucleus is roughly four bonds from the binding site of the lanthanide (e.g., $\text{Ln}-\text{O}-\text{W}-\text{O}-\text{P}$), and approximately 4.5 Å through open space from the lanthanide ion (based on reported crystal structures for M^{3+} - $\text{PW}_{11}\text{O}_{39}^{7-}$ complexes).^{35,39} Considering that the Fermi-contact shift is due to the delocalization of paramagnetic electrons from the lanthanide to the NMR nucleus through bonds, it is an unlikely contribution to the shift observed for paramagnetic Ln^{3+} -POM chemical shifts. The dipolar shift or

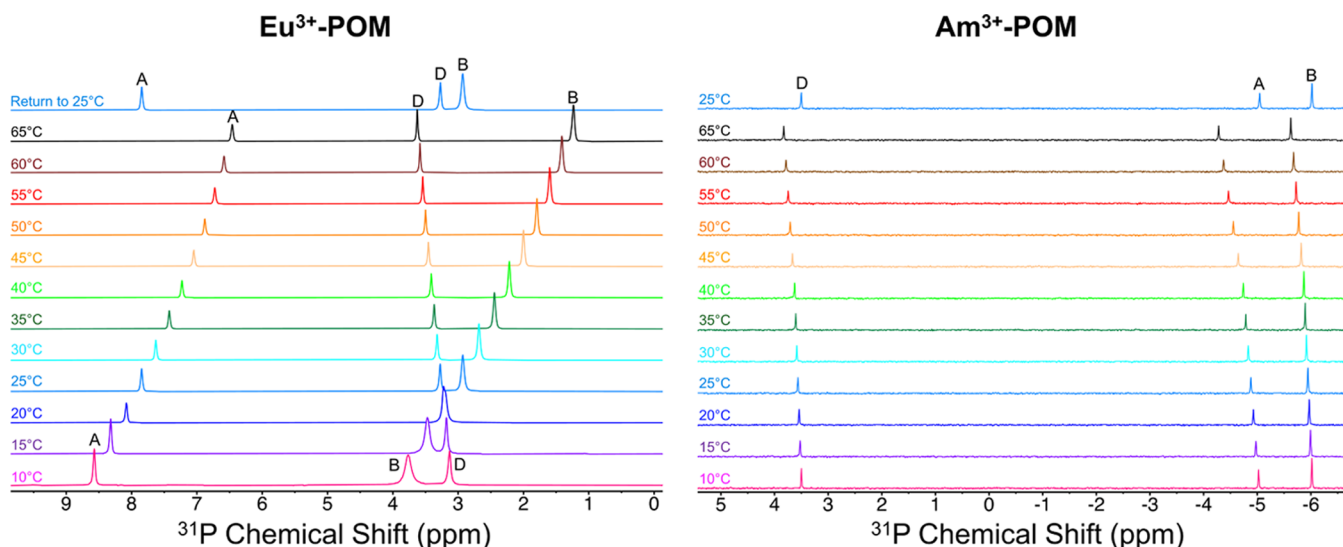


Figure 4. ^{31}P VT-NMR spectra of the $\text{Eu}^{3+}\text{-PW}_{11}\text{O}_{39}^{7-}$ (left) and $\text{Am}^{3+}\text{-PW}_{11}\text{O}_{39}^{7-}$ (right) complexes in solution. The peaks, labeled D, A, and B, in the $\text{Eu}^{3+}\text{-PW}_{11}\text{O}_{39}^{7-}$ spectra on the left correspond to unchelated phosphate ions present in the buffer (D), the $\text{Eu}(\text{POM})$ complex (A), and $\text{Eu}(\text{POM}_2)$ (B). Signals D and B cross paths at 20 °C and change their relative positions in the spectrum above 20 °C. (Right) Comparative results for the $\text{Am}^{3+}\text{-PW}_{11}\text{O}_{39}^{7-}$ system. Results for the other lanthanides (La, Sm, Nd, Yb, and Lu) and $\text{Cm}^{3+}\text{-PW}_{11}\text{O}_{39}^{7-}$ are shown in Figures S6–S10. Chemical shift values and peak areas as a function of temperature for $\text{Eu}^{3+}\text{-POM}$ are provided in Figure S11. Peak areas for all $M^{3+}\text{-POM}$ complexes as a function of temperature are provided in Table S3. Corresponding chemical shifts are given in Table S1.

pseudo-contact shift is likely responsible and employs the largest effect on chemical shifts in the complexes studied here. While it is theoretically possible to separate out the two contributions to the paramagnetic chemical shift, this type of evaluation is well beyond the scope of this manuscript.

The spectra of the $\text{Am}^{3+}\text{-POM}$ and $\text{Cm}^{3+}\text{-POM}$ samples (Figure 2) exhibit similar features as their $\text{Ln}^{3+}\text{-POM}$ counterparts, with three NMR signals, one from the free phosphate ions at 3.4 ppm (peak D) and two upfield signals (peaks A and B) corresponding to the actinide-POM species. Despite their radioactive nature, the stability of the actinide-POM complexes in solution is quite robust. Long-term stability experiments showed that the NMR spectrum of the $^{243}\text{Am}^{3+}\text{-POM}$ complexes (the sample with highest specific activity, ~4 GBq/L, including α and γ emission from $^{243}\text{Am}^{3+}$ and β^- emission from the short-lived daughter ^{239}Np , in secular equilibrium) remains unchanged over a period of at least 2 months and even after prolonged warming–cooling cycles up to 65 °C (Figure S4). We hypothesize that the inorganic nature of the POMs and the ability to assemble from smaller building blocks (e.g., WO_4^{2-}) render them inherently more resistant to radiolytic damage than organic chelators (which are prone to oxidation and degradation in the presence of actinides)^{75–77} since breaking of bonds in the $\text{PW}_{11}\text{O}_{39}^{7-}$ structure would be followed by reassembly of the POM. Consistent with the behavior observed for the actinide-POM solutions, solutions of lanthanide-POM complexes or unbound POM are also stable for extended periods of time (i.e., at least several weeks, Figure S5).

Further analysis of the chemical shift values of peaks A and B with respect to cation composition (Figure 3a) demonstrates that these peaks are highly correlated, supporting the hypothesis that these peaks represent two stable species in equilibrium with one another. Peaks A and B of the two POM complexes are further upfield in the case of curium compared to americium: -5.09 and -6.05 ppm for $[\text{Am}^{\text{III}}(\text{PW}_{11}\text{O}_{39}^{7-})(\text{H}_2\text{O})_x]^{4-}$ and $[\text{Am}^{\text{III}}(\text{PW}_{11}\text{O}_{39}^{7-})_2]^{11-}$ vs -8.87, and -9.40

ppm for $[\text{Cm}^{\text{III}}(\text{PW}_{11}\text{O}_{39}^{7-})(\text{H}_2\text{O})_x]^{4-}$ and $[\text{Cm}^{\text{III}}(\text{PW}_{11}\text{O}_{39}^{7-})_2]^{11-}$, respectively. Interestingly, the NMR signals of the actinide-POM complexes exhibit greater chemical shift separation than those of the corresponding diamagnetic lanthanide complexes (La, Lu). However, the peak separation is smaller than those of paramagnetic Ln-POM complexes (Nd, Eu, Yb). This trend suggests that Am^{3+} and Cm^{3+} ions in solution are weakly paramagnetic (Figure 3b). This observation was also confirmed by the relaxation time measurements (vide infra).

Interestingly, in prior NMR studies performed on $^{241}\text{Am}^{3+}$ and $^{244}\text{Cm}^{3+}$ in unchelating media (1 M HClO_4 solutions),^{63,65} and that used the Evans method,⁷⁸ it was found that the 9-coordinated $[\text{Cm}(\text{H}_2\text{O})_9]^{3+}$ ion is far more paramagnetic than the $[\text{Am}(\text{H}_2\text{O})_9]^{3+}$ ion, with magnetic susceptibility of the curium samples being ~25× higher than that of the americium samples. Such a strong difference is not manifested in the NMR properties of the POM complexes described in the present study, where the paramagnetism of the $^{248}/^{246}\text{Cm}^{3+}$ complexes with $\text{PW}_{11}\text{O}_{39}^{7-}$ appear almost on par with their $^{243}\text{Am}^{3+}$ counterparts. This apparent discrepancy is likely a result of the particular coordination mode of the actinide in the $\text{PW}_{11}\text{O}_{39}^{7-}$ complexes, which are 8-coordinated (as supported by single-crystal XRD structures³⁹). The POM anions also induce a strong ligand field (compared to water molecules or organic ligands) and likely affect the electronic ordering of the chelated actinide ion. These NMR observations are in line with our prior fluorescence measurements³⁹ (which probes the electronic excited and ground states of the actinide) that showed that 8-coordinated $\text{Cm}^{3+}\text{-POM}$ complexes exhibit behaviors that depart from the previously characterized 9-coordinated complexes.

Finally, it should be underlined that the characterization approach demonstrated here, which combines the POM chelating platform with NMR spectroscopy, enables both the direct observation of the chemical species present and the indirect observation of the magnetic properties of these

transuranic elements. Efforts are ongoing to extend our POM–NMR approach to other rare radioelements such as promethium, actinium, or transcurium actinides.^{54,79–81}

Variable-Temperature ^{31}P NMR of Ln–POM and An–POM Complexes. Variable-temperature NMR experiments were performed to gain further insights into the interactions between POMs and f-block metal ions. VT-NMR experiments provide insight into the temperature dependence of nuclear shielding and can help elucidate chemical speciation. In this case, VT-NMR was conducted to calculate thermodynamic parameters for the equilibrium reaction between 1:1 and 1:2 cation–POM complexes in solution. The series of VT-NMR spectra for all of the actinide and lanthanide solutions studied here (Am^{3+} , Cm^{3+} , La^{3+} , Nd^{3+} , Sm^{3+} , Eu^{3+} , Yb^{3+} , and Lu^{3+} , complexed to $\text{PW}_{11}\text{O}_{39}^{7-}$) are compiled in the Supporting Information (Figures S6–S10). Figure 4 contrasts the VT-NMR spectra of the Eu^{3+} –POM and Am^{3+} –POM systems. The europium and americium systems are compared here as Eu^{3+} is often taken as a nonradioactive surrogate for Am^{3+} since both elements are in the same column of the periodic table and have relatively similar ionic radii.⁷¹ However, the present NMR results show that the Eu^{3+} –POM and Am^{3+} –POM complexes have distinct solution chemistry. Among the trivalent f-element species studied here, the nuclear shielding of the 1:1 and 1:2 Eu –POM complexes have the greatest temperature dependence, shifting by almost 3 ppm from 10 to 65 °C, and contrast with the Am–POM (and Cm–POM) counterparts. Figure 4 (left) shows the NMR signatures associated with the $[\text{Eu}^{\text{III}}(\text{PW}_{11}\text{O}_{39})(\text{H}_2\text{O})_x]^{4-}$ (peak A) and $[\text{Eu}^{\text{III}}(\text{PW}_{11}\text{O}_{39})_2]^{11-}$ (peak B) complexes in phosphate-containing buffer as a function of temperature, from 10 to 65 °C. At 20 °C, peaks B and D (free phosphate ions) look to coalesce but are more likely swapping positions since they separate again at $T > 20$ °C. Unlike the VT-NMR spectra of Eu–POMs, signals in spectra of Am–POMs (Figure 4, right) do not cross paths but do slightly shift downfield (by ~1 ppm) with increasing temperature.

Based on the peak area distribution (Table S3), the apparent reaction constant (K_{app}) corresponding to the conversion of the 1:1 complex to the 1:2 complex, for each metal, was estimated (see the Materials and Methods Section, eqs 1–4). The repartition between the 1:1 and 1:2 complexes as a function of the temperature, as observed by ^{31}P VT-NMR, can also be used to calculate the reaction enthalpy (ΔH_{rxn}) and entropy (ΔS_{rxn}) of the interconversion equilibrium. Table 1 summarizes the thermodynamic parameters derived from the NMR experiments on the lanthanide–POM and actinide–POM complexes.

Interestingly, under the studied conditions and at 25 °C, all of the studied lanthanides favor the 1:1 complex, $[\text{Ln}^{\text{III}}(\text{PW}_{11}\text{O}_{39})(\text{H}_2\text{O})_x]^{4-}$, with $\text{Ln } K_{\text{app}} < 1$. The early lanthanides (La, Nd, Sm) strongly favor the formation of the 1:1 complex, $[\text{Ln}^{\text{III}}(\text{PW}_{11}\text{O}_{39})(\text{H}_2\text{O})_x]^{4-}$, whereas Eu^{3+} and Lu^{3+} form the 1:2 complex $[\text{Ln}^{\text{III}}(\text{PW}_{11}\text{O}_{39})_2]^{11-}$ in concentration relatively similar to its 1:1 counterpart. For actinides, analysis of the NMR spectra indicates that both Am^{3+} and Cm^{3+} favor the 1:1 complex, albeit with Am^{3+} forming the 1:2 complex in slightly higher concentration than Cm^{3+} . It should be noted that for all of the metals studied here, relatively modest interconversion equilibrium constants were observed, and both complexes persist in solution in significant proportions (i.e., each complex representing ~10 to ~90% of the total metal speciation). This result would not be expected

Table 1. Thermodynamic Parameters (Apparent Constant of Reaction, $\text{Ln } K_{\text{app}}$ at 298 K, Reaction Enthalpy, ΔH_{rxn} , and Entropy, ΔS_{rxn}) Calculated Based on the NMR Peak Areas and VT-NMR Experiments^a

ion	$\text{Ln } K_{\text{app}}$ (298 K)	ΔH_{rxn} (kJ/mol)	ΔS_{rxn} (J/mol)
La^{3+}	-3.36	0.602	-25.9
Nd^{3+}	-2.91	-0.449	-25.7
Sm^{3+}	-3.16	0.558	-24.4
Eu^{3+}	0.60	-1.26	0.79
Lu^{3+}	-0.387	-18.1	-63.9
Am^{3+}	-0.11	-5.85	-20.5
Cm^{3+}	-1.25	0.26	-9.53

^aThe reaction corresponds to the formation of the 1:2 metal/POM complex from the 1:1 complex, i.e., $\text{M(POM)} + \text{POM} = \text{M(POM)}_2$. Thermodynamic values were calculated using the Van't Hoff equation. The Van't Hoff plots for the individual metal/POM systems are given in Figures S12–S17. pH = 4.5. I = 0.1 M. POM = $\text{PW}_{11}\text{O}_{39}^{7-}$.

for the $[\text{M}^{\text{III}}(\text{PW}_{11}\text{O}_{39})(\text{H}_2\text{O})_x]^{4-}$ species as half of the metal-ion coordination sphere is exposed to solvent molecules or open to attack by other ligands. This means that the $\text{PW}_{11}\text{O}_{39}^{7-}$ is a strong enough chelator to prevent the metal hydrolysis (and, under the conditions of this study, precipitation with free phosphate ions), even when forming complexes that do not completely fill the metal coordination sphere. This kind of speciation, where the different metal:POM species are in equilibrium with relatively similar apparent thermodynamic stability, could be beneficial for potential separation applications as subtle differences among the metals could lead to the formation of either the 1:1 or the 1:2 complex, giving leverages for distinct extraction or precipitation behaviors.

The VT-NMR experiments also shed light on the effect of temperature on nuclear shielding. The nuclear shielding of signal D (free phosphate) shown in Figure 4 is not as temperature-dependent as the POM species corresponding to signals A and B. This observation suggests that the extent of nuclear shielding of the phosphate ion encapsulated in the POM ligand is highly sensitive to the electronic structure of the Ln–POM complex, which is a function of the pseudo-contact shift.⁷³

Among the metal/POM systems studied, Lu^{3+} is the most sensitive to temperature, as illustrated in Figure 5. Even within the relatively limited temperature range compatible with aqueous samples, we could observe an almost complete reversal of the distribution of the Lu/POM species, with the $[\text{Lu}^{\text{III}}(\text{PW}_{11}\text{O}_{39})_2]^{11-}$ complex being predominant at $T \leq 40^\circ\text{C}$, while the $[\text{Lu}^{\text{III}}(\text{PW}_{11}\text{O}_{39})(\text{H}_2\text{O})_x]^{4-}$ complex becomes predominant at $T \geq 40^\circ\text{C}$. Such a drastic sensitivity to temperature could be used for temperature-controlled isolation of the individual complexes. The corresponding Van't Hoff plot (Figure 5) indicates an exothermic formation of $[\text{Lu}^{\text{III}}(\text{PW}_{11}\text{O}_{39})_2]^{11-}$ from $[\text{Lu}^{\text{III}}(\text{PW}_{11}\text{O}_{39})(\text{H}_2\text{O})_x]^{4-}$ (peak A), with $\Delta H_{\text{rxn}} = -18.1$ kJ/mol. For the other metal:POMs tested, the reaction conversion between the 1:1 and 1:2 complexes have very low reaction enthalpies and are close to athermicity, with $\Delta H_{\text{rxn}} \leq 3$ kJ/mol, in the temperature range investigated. The ΔH_{rxn} values for Am–POM and Cm–POM complexes fall within the range observed for the lanthanide complexes with the interconversion reaction of both actinides being slightly exothermic.

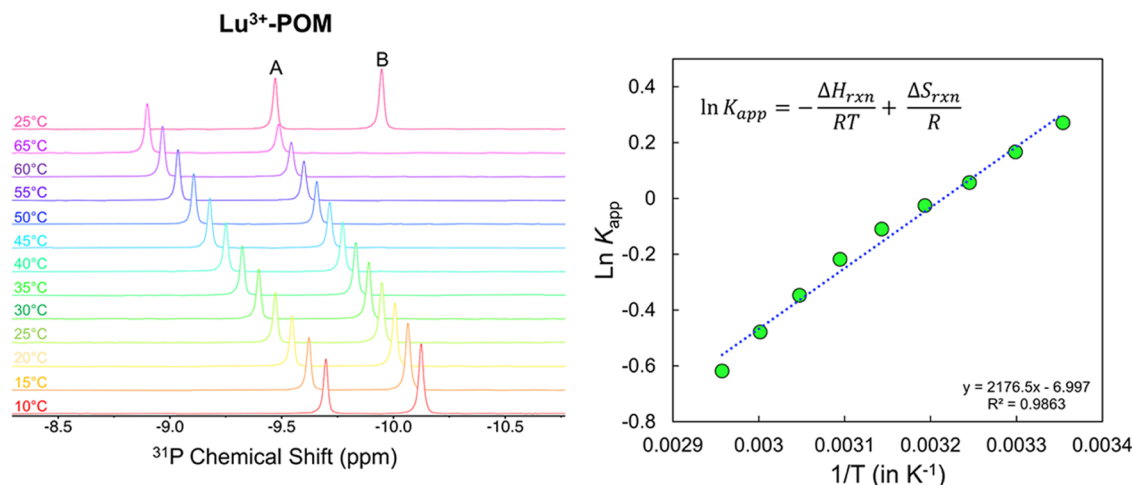


Figure 5. (Left) VT-NMR spectra corresponding to the $\text{Lu}(\text{PW}_{11})$ and $\text{Lu}(\text{PW}_{11})_2$ complexes. (Right) Van't Hoff plot used to determine the reaction enthalpy and entropy for the equilibrium reaction between the $\text{Lu}(\text{PW}_{11})$ and $\text{Lu}(\text{PW}_{11})_2$ complexes. Values of $\ln K_{app}$ were determined from integrated peak areas of peaks A and B in the temperature range of 25–50 °C. See Table 1 for corresponding thermodynamic parameters of the other lanthanide–POM and actinide–POM systems studied.

Relaxometry Measurements on Ln–POM and An–POM Complexes. NMR spectroscopy was also used to measure the spin-lattice relaxation times (T_1) of the POM complexes in solution. To the best of our knowledge, this technique has not been used before for americium or curium species, which gives another tool to study the solution chemistry and dynamics of these rare elements. T_1 values at 25 °C were determined for all actinide–POM and lanthanide–POM complexes studied herein, i.e., $[\text{M}(\text{PW}_{11}\text{O}_{39})(\text{H}_2\text{O})_x]^{4-}$ and $[\text{M}(\text{PW}_{11}\text{O}_{39})_2]^{11-}$ ($\text{M} = {}^{243}\text{Am}^{3+}, {}^{248/246}\text{Cm}^{3+}, \text{La}^{3+}, \text{Nd}^{3+}, \text{Sm}^{3+}, \text{Eu}^{3+}, \text{Yb}^{3+}, \text{Lu}^{3+}$). The T_1 results are summarized in Table 2, and the full T_1 build-up curves, for the 1:1 and 1:2 complexes with each metal, are shown in Figures S18–S25.

The measured T_1 values for the Ln–POM complexes range from milliseconds to seconds, with the shortest corresponding to complexes with paramagnetic lanthanides. The longest T_1 values are observed in the case of POM complexes of

Table 2. Spin-Lattice Relaxation Times (T_1) and Chemical Shifts for the 1:1 Complex ($[\text{M}^{III}(\text{PW}_{11}\text{O}_{39})(\text{H}_2\text{O})_x]^{4-}$; Identified as Peak A in the NMR Spectra Shown in Figure 2) and 1:2 Complex ($[\text{M}^{III}(\text{PW}_{11}\text{O}_{39})_2]^{11-}$; Identified as Peak B in Figure 2) as a Function of Lanthanide or Actinide Ion^a

metal ion	T_1 of 1:2 metal–POM complex (in s)	chemical shift for the 1:2 complex (ppm)	T_1 of 1:1 metal–POM complex (s)	chemical shift for the 1:1 complex (ppm)
La^{3+}	14.00	-8.89	12.20	-8.62
Nd^{3+}	0.15	-21.47	0.10	-19.74
Sm^{3+}	3.40	-12.22	2.55	-11.84
Eu^{3+}	0.18	3.01	0.27	7.91
Yb^{3+}	0.04 ^b	31.85	0.03 ^b	37.40
Lu^{3+}	12.10	-9.94	18.50	-9.46
Am^{3+}	7.00	-6.05	10.31	-5.09
Cm^{3+}	9.04	-9.40	12.22	-8.87

^aThe unchelated PW_{11} cluster has a T_1 of 23.0 s and has a chemical shift of -7.44 ppm. Free phosphate ions present in the same buffer and without f-elements exhibit a T_1 value of ~9 s. T_1 measurements were conducted at 25 °C. ^bGiven the short values of these two T_1 's and subsequent sensitivity of fitting the T_1 build-up curves, we estimate these times at ± 5 ms.

diamagnetic lanthanide ions (La^{3+} and Lu^{3+}), with T_1 relaxation times of 14 to 19 s. This compares to a T_1 of 23 s for the solutions of the POM without metal ions, which further confirms the complexation of the POM to the f-block cations. T_1 measurements for the phosphate ions present in the buffer solution (peak D at 3.4 ppm in ^{31}P NMR spectra) revealed a T_1 value of ~9 s, regardless of the presence of the f-element (Table S2), which further confirms that f-elements were prevented from interacting with phosphate ions due to complexation to the POM.

In the case of paramagnetic solutions, the unpaired electrons of the paramagnetic lanthanides have very short relaxation times, which affects the relaxation time of the neighboring ^{31}P nucleus through space and bonds. This effect was observed for all paramagnetic lanthanide ions studied here, with T_1 values of only ~3 s for the Sm^{3+} -POM complexes, 100–300 ms for both Nd^{3+} -POM and Eu^{3+} -POM, and just ~35 ms for the Yb^{3+} -POM species (Table 2). In the case of americium and curium species, the T_1 values are intermediate to that of diamagnetic lanthanides and paramagnetic lanthanides, with 7.0 and 10.3 s for the Am^{3+} -POM complexes and 9.0 and 12.2 s for their Cm^{3+} -POM counterparts (Table 2). These relaxometry results confirm the trend observed for the chemical shifts (vide supra, Figure 3) where trivalent americium and curium behave as weakly paramagnetic ions, with a slightly more pronounced paramagnetic character for curium relative to americium. It is important to emphasize that the combined use of POMs and NMR spectroscopy facilitates the observation of this property of these transplutonium actinide ions. Performing similar ^{31}P NMR measurements on simple phosphate solutions of actinides would be impractical due to the low solubility of f-elements/phosphate complexes ($\text{pK}_s \approx 25$)⁷² and large excess of ligand needed to form them,^{82,83} whereas the encapsulation of PO_4^{3-} in $\text{PW}_{11}\text{O}_{39}^{7-}$ allows for the formation of highly soluble and stable actinide and lanthanide complexes, including in the presence of phosphate ions in the buffer. Our POM–NMR approach could be extended to other NMR-active nuclei that can be encapsulated in POMs similar to $\text{PW}_{11}\text{O}_{39}^{7-}$ (e.g., ${}^{10/11}\text{B}$, ${}^{75}\text{As}$, ${}^{77}\text{Se}$, and ${}^{29}\text{Si}$).

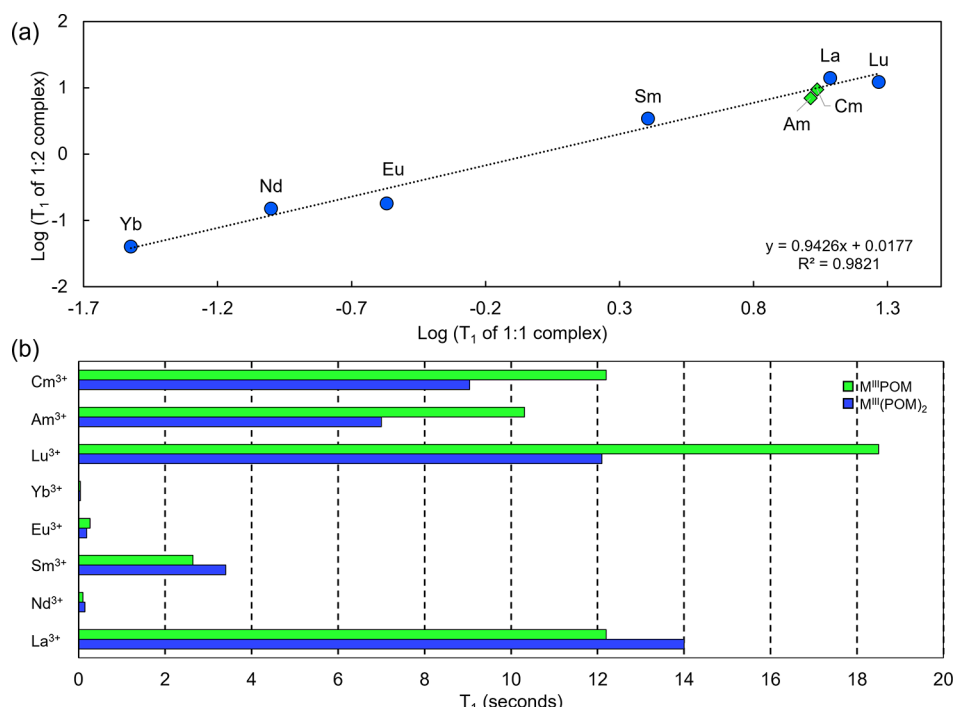


Figure 6. (a) Correlation between the T_1 values of the two POM complexes, $M(PW_{11})$ and $M(PW_{11})_2$, with actinides and lanthanides. Note that the logarithmic scale is used in this plot since the T_1 times span 3 orders of magnitude. (b) Comparison of the T_1 values measured for the two complexes for trivalent lanthanides and actinides. Notice the short T_1 values for all of the paramagnetic lanthanides studied here, which have T_1 values on the order of milliseconds. Green bars correspond to the 1:1 complex, and blue bars correspond to the 1:2 complex. It is also worth noting the reversal of T_1 values across the lanthanide series where, prior to Eu^{3+} , T_1 values of the 1:2 complexes are longer than that of the 1:1 complex, while after Eu^{3+} , T_1 's are shorter for the 1:2 complex, including Yb^{3+} . For numerical T_1 values, the reader is directed to Table 1. T_1 times corresponding to free phosphate ions in the buffer of the actinide-POM and lanthanide-POM samples are tabulated in Table S2.

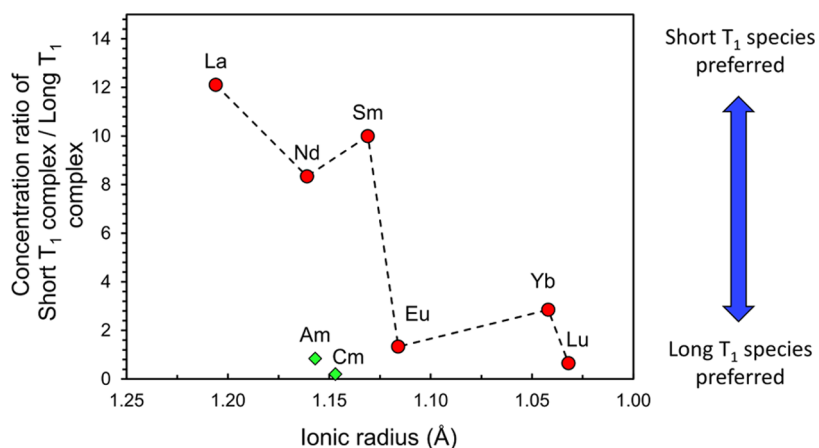


Figure 7. Comparison of the concentration ratio of the complexes (short T_1 species/long T_1 species) along the trivalent lanthanide and actinide series. Concentrations were calculated based on peak areas and the stoichiometry of the complexes. T_1 times and peak areas were measured at $T = 25\text{ }^\circ\text{C}$. The red circles correspond to lanthanides, and the green diamonds correspond to americium and curium. Ionic radius values were taken from the studies by Lundberg and co-workers.^{71,84}

As highlighted in Figure 6a, the T_1 values of the lanthanide-POM and actinide-POM complexes span ~ 3 orders of magnitude but, for each metal, the two T_1 values are highly correlated, further suggesting that the two observed NMR peaks belong to relatively similar species in equilibrium. Figure 6b details the T_1 values observed for the different 1:1 and 1:2 complexes with lanthanides and actinides. The longest T_1 times observed correspond to solutions of Lu-POM, with a 1:1 complex T_1 time of 18.5 s and a 1:2 complex T_1 time of 12.1 s. The shortest T_1 times correspond to solutions of Yb-

POM, with a 1:1 cluster T_1 time of 0.04 s and a 1:2 cluster T_1 time of 0.03 s. The T_1 times of Am-POMs and Cm-POMs are surprisingly similar, and of similar magnitude but shorter than the Lu-POMs. Interestingly, the order of the T_1 times of the two types of metal-POM complexes (i.e., 1:1 and 1:2 species) reverses as we cross the lanthanide series, with an inflection near Eu. Indeed, the 1:1 complex has a shorter T_1 than the 1:2 complex in the case of La^{3+} , Nd^{3+} , and Sm^{3+} , but the opposite is observed for the heavier lanthanides. T_1 values of Am-POM and Cm-POM samples indicate that their 1:1

complexes exhibit longer T_1 values than their respective 1:2 complexes, similar to the late lanthanides.

Interestingly, as shown in Figure 7, comparing the distribution of the two complexes for each metal/POM system reveals that species with longer T_1 times predominate for the early lanthanides, while the species with shorter T_1 times predominate for the late lanthanides, with an apparent break at Eu. To the best of our knowledge, such an effect was not observed before for f-element complex series. It should be noted that such an observation was only possible due to a fortunate combination of factors that include the formation of multiple complexes that coexist in the f-element/POM systems, the presence of an NMR-active nucleus (^{31}P), and the use of multiple NMR techniques to identify the species and measure their nuclear spin-lattice relaxation times. The results for americium and curium also allude that there exists a similar trend, albeit specific to the actinide series. However, other actinide ions (i.e., Ac^{3+} , Pu^{3+} , Bk^{3+} , Cf^{3+} , etc.) will need to be probed via our POM–NMR approach to confirm this observation. Future efforts will focus on expanding our approach to other actinide–POM and lanthanide–POM systems.

The combined analysis of signal ratios/positions and T_1 times shows that it is possible to effectively speciate f-element samples without more complicated NMR investigations, such as diffusion-ordered spectroscopy (DOSY),⁸⁵ which may be out of reach for radioactive and/or diluted samples. This method is potentially a new way of using NMR to understand the chemical behavior and speciation of POMs incorporating rare ions. To further decipher the bonding interactions into these heavy element–POM complexes, chemical shift calculations using *ab initio* methods are currently being performed and will be reported on in a later communication.

CONCLUSIONS

This study represents the first investigation of the solution-state chemistry of americium and curium–POM complexes using NMR spectroscopy, including 1D ^{31}P NMR, VT-NMR, and T_1 measurements. The intrinsic properties of the heteropolyoxotungstate POM ligands yield a convenient platform to study complexes of actinide and lanthanide ions in solution using ^{31}P NMR spectroscopy, even when using microgram amounts and in phosphate solutions where f-elements are typically insoluble. The concurrent formation of two complexes, $[\text{M}^{\text{III}}(\text{PW}_{11}\text{O}_{39})(\text{H}_2\text{O})_x]^{4-}$ and $[\text{M}^{\text{III}}(\text{PW}_{11}\text{O}_{39})_2]^{11-}$, was observed for all trivalent lanthanides and actinides tested (M = La, Nd, Sm, Eu, Yb, Lu, Am, Cm). The observed chemical shifts and T_1 measurements indicate a weak paramagnetic behavior for Am^{3+} and Cm^{3+} in solution. The NMR results also reveal a reversal of the T_1 values of the 1:1 and 1:2 complexes along the lanthanide series and the existence of a potentially similar trend for trivalent actinides. This work shows that the combination of tailored ligands such as POMs containing NMR-active nuclei can facilitate the study of rare, expensive, and/or toxic isotopes such as those of transplutonium elements.

MATERIALS AND METHODS

Caution! ^{243}Am (half-life = 7,388 years; specific activity = 14.8 GBq/g, including the ^{239}Np decay product in secular equilibrium) and $^{248}/^{247}\text{Cm}$ isotopes (^{248}Cm half-life = 3.49×10^5 years; specific activity = 0.16 GBq/g) constitute serious health hazards because of their radioactive and chemical properties. ^{243}Am and ^{248}Cm samples

require special safety protocols, personal protective equipment, and facilities since these isotopes are α , γ , and neutron emitters, and undergo spontaneous fissions. All experiments involving radionuclides were conducted at Lawrence Livermore National Laboratory, in facilities designed for the safe handling of long-lived and short-lived radioactive materials and associated waste.

Materials. All solutions were prepared using deionized water purified by reverse osmosis cartridge system ($\geq 18.2 \text{ M}\Omega\cdot\text{cm}$). Na_2HPO_4 ($\geq 99\%$), NaCH_3COO ($\geq 99.9\%$), $\text{Na}_2\text{WO}_4 \cdot 2\text{H}_2\text{O}$ ($\geq 99\%$), phosphoric acid, lanthanide trichloride salts ($>99.9\%$), and deuterated water (>99 atom %D) were purchased from chemical providers (VWR and MilliporeSigma) and used as received. The pH of the solutions was adjusted via additions of micro-amounts of standard solutions of HCl or NaOH (VWR). The precursor for the $\text{PW}_{11}\text{O}_{39}^{7-}$ ion, namely, $\text{Na}_9\text{PW}_9\text{O}_{39} \cdot 7\text{H}_2\text{O}$, was synthesized according to a literature procedure.⁶⁷ Briefly, the $\text{Na}_9\text{PW}_9\text{O}_{39} \cdot 7\text{H}_2\text{O}$ salt was prepared by dissolving 12 g of $\text{Na}_2\text{WO}_4 \cdot 2\text{H}_2\text{O}$ in 15 mL of H_2O . A small volume of 85% H_3PO_4 was added dropwise ($\sim 400 \mu\text{L}$) to form the POM and the pH was then adjusted to 7–7.5 with glacial acetic acid (2.25 mL). During the addition of acetic acid, a precipitate immediately forms. The solid-solution slurry was stirred for an hour, and the solid was then filtered under vacuum. The PW_9 POM is unstable in solution at a pH of 4.5 (studied conditions) and converts to PW_{11} upon binding to the trivalent lanthanide or actinide ions. The actinide samples were prepared by dilution of primary stock solutions made from primary sources of $^{243}\text{Am}(\text{III})$ or $\text{Cm}(\text{III})$ (97% ^{248}Cm + 3% ^{246}Cm + 0.01% ^{247}Cm) purchased from Oak Ridge National Laboratory.

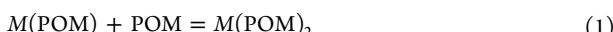
NMR Sample Preparation. Metal/POM complexes were prepared *in situ*. The $\text{Na}_9\text{PW}_9\text{O}_{39} \cdot 7\text{H}_2\text{O}$ precursor was dissolved in a 100 mM NaCH_3COO buffer at pH 4.5, containing 2 mM Na_2HPO_4 .

For each lanthanide or actinide, an aliquot of a metal(III) chloride stock solution was added to the POM solution in stoichiometric amounts (ratio of 1:2 between the studied metal ion and the POM). An aliquot of D_2O was then added so that the final NMR sample contained 25% D_2O . The samples were equilibrated at room temperature for at least 2 h before NMR measurements. Samples were prepared under ambient atmosphere. Metal concentrations in the samples were 4 mM for lanthanides and 1 mM for actinides. Control experiments with the lanthanide/POM samples at different concentrations showed no change in the NMR spectra in this concentration range. For actinides, due to safety precautions inherent to work with radioactive materials, the samples were transferred into a PTFE liner (volume of sample = 300 μL) to create doubly contained NMR samples. Sample preparation and NMR measurements were performed at LLNL in laboratories specifically designed for work with liquid samples containing long-lived α emitters. The stability of the samples over time was monitored, as shown in Figures S4–S5. Following VT-NMR measurements (up to 65 °C), additional NMR spectra were measured after cooling down the samples back to 25 °C to verify the reversibility of the temperature-induced reactions. Following NMR data collection, the actinide materials were recovered and recycled for other studies.

NMR Spectroscopy. All NMR spectroscopic experiments were conducted at the Center for National Security Applications of Magnetic Resonance at LLNL. Solution-state ^{31}P NMR spectroscopy was conducted using both 500 and 600 MHz on Bruker Avance III spectrometers at 11.74 and 14.10 T, respectively. The operating frequency for ^{31}P is 202.457 and 242.938 MHz on 500 and 600 MHz instruments, respectively. An external standard of 85% phosphoric acid solution in 90% H_2O with 10% D_2O was referenced to 0 ppm. A 90° pulse width was calibrated before each experiment and varied between 11.8 and 12.5 μs . In general, 1D ^{31}P NMR experiments were done using inverse-gated proton decoupling to ensure quantitative results. Data collected on the 500 MHz instrument used a Bruker Prodigy cryoprobe for greater sensitivity and less background interference. Spin-lattice relaxation experiments to determine T_1 times of the molecular species utilized the inversion recovery method.

All 1D and T_1 experiments were conducted at 25 °C unless otherwise noted as in the variable-temperature experiments.

VT-NMR experiments were conducted in the same manner as 1D experiments in the temperature range of 10–65 °C for lanthanide samples and 25–65 °C for samples with $^{248/246}\text{Cm}^{3+}$ and $^{243}\text{Am}^{3+}$. In all cases, after the VT series were completed, the sample was returned to 25 °C and a spectrum was collected. The series of VT-NMR spectra are included in the Supporting Information (Figures S6–S10) as well as Figures 4 and 5. VT-NMR results were used to extract thermodynamic parameters for the equilibrium reaction between the 1:1 and 1:2 complexes studied here. The NMR peak areas were used to determine the distribution of the two species. The following reaction equilibrium was considered



where M is a trivalent actinide or lanthanide cation, and POM is the $\text{PW}_{11}\text{O}_{39}^{7-}$ ligand. The associated apparent formation reaction constant under the studied conditions, K_{app} , is

$$K_{\text{app}} = \frac{[\text{M(POM)}_2]}{[\text{M(POM)}] \times [\text{POM}]} \quad (2)$$

Since the study was performed with stoichiometric samples (i.e., 1:2 ratio between the studied f-element and the POM), no free metal is expected in solution. If the 1:2 complex dissociates, it forms an equal quantity of 1:1 complex and free POM. Therefore, the concentrations of free POM and 1:1 complex in solution are equal and the following equation is obtained.

$$K_{\text{app}} = \frac{[\text{M(POM)}_2]}{[\text{M(POM)}]^2} \quad (3)$$

As the NMR peak areas are proportional to the species concentration, one can therefore estimate K_{app} , based on the ^{31}P NMR spectra. Moreover, the VT-NMR spectra were used to calculate the reaction enthalpy (ΔH_{rxn}) and entropy (ΔS_{rxn}), using the Van't Hoff equation, as written below.

$$\ln K = -\frac{\Delta H_{\text{rxn}}}{RT} + \frac{\Delta S_{\text{rxn}}}{R} \quad (4)$$

Van't Hoff plots, where $\ln K_{\text{app}}$ is plotted against the inverse of the temperature, constructed for the metal/POM complexes studied here are shown in Figure S12–S17.

ASSOCIATED CONTENT

Supporting Information

The Supporting Information is available free of charge at <https://pubs.acs.org/doi/10.1021/acs.inorgchem.2c04014>.

Pictures of curium–POM sample; control ^{31}P NMR spectra with buffer and unchelated POM; NMR spectra of actinide and lanthanide samples over time; ^{31}P VT-NMR for actinide–POM and lanthanide–POM samples and corresponding Van't Hoff plots; T_1 buildup curves for actinide–POM and lanthanide–POM complexes; T_1 values for the free phosphate ions present in the buffer, and chemical shifts as a function of temperature (PDF)

AUTHOR INFORMATION

Corresponding Author

Gauthier J.-P. Deblonde – Glenn T. Seaborg Institute, Physical and Life Sciences Directorate and Nuclear and Chemical Sciences Division, Lawrence Livermore National Laboratory, Livermore, California 94550, United States; orcid.org/0000-0002-0825-8714; Email: deblonde1@llnl.gov

Authors

Christopher A. Colla – Atmospheric, Earth and Energy Division, Lawrence Livermore National Laboratory, Livermore, California 94550, United States; orcid.org/0000-0002-2095-3752

Ian Colliard – Glenn T. Seaborg Institute, Physical and Life Sciences Directorate, Lawrence Livermore National Laboratory, Livermore, California 94550, United States; Department of Chemistry, Oregon State University, Corvallis, Oregon 97331, United States; orcid.org/0000-0003-1883-1155

April M. Sawvel – Materials Science Division, Lawrence Livermore National Laboratory, Livermore, California 94550, United States; orcid.org/0000-0002-8810-807X

May Nyman – Department of Chemistry, Oregon State University, Corvallis, Oregon 97331, United States; orcid.org/0000-0002-1787-0518

Harris E. Mason – Atmospheric, Earth and Energy Division, Lawrence Livermore National Laboratory, Livermore, California 94550, United States; Chemistry Division, Los Alamos National Laboratory, Los Alamos, New Mexico 87545, United States; orcid.org/0000-0002-1840-0550

Complete contact information is available at:

<https://pubs.acs.org/10.1021/acs.inorgchem.2c04014>

Notes

The authors declare no competing financial interest.

ACKNOWLEDGMENTS

This work was performed under the auspices of the U.S. Department of Energy (DOE) by Lawrence Livermore National Laboratory under Contract DE-AC52-07NA27344 and was supported by the LDRD Program under the LLNL project 20-LW-017. Release number: LLNL-JRNL-837416. M.N. and I.C. also acknowledge support from the Department of Energy, National Nuclear Security Administration under Award DENA0003763. The authors thank Dr. Mavrik Zavarin (LLNL) for supporting this project and for fruitful discussions. G.J.-P.D. thanks S. Peters for interesting discussions.

REFERENCES

- (1) Gumerova, N. I.; Rompel, A. Polyoxometalates in Solution: Speciation under Spotlight. *Chem. Soc. Rev.* **2020**, *49*, 7568–7601.
- (2) Blazevic, A.; Rompel, A. The Anderson–Evans Polyoxometalate: From Inorganic Building Blocks via Hybrid Organic–Inorganic Structures to Tomorrows “Bio-POM”. *Coord. Chem. Rev.* **2016**, *307*, 42–64.
- (3) Misra, A.; Kozma, K.; Streb, C.; Nyman, M. Beyond Charge Balance: Counter-Cations in Polyoxometalate Chemistry. *Angew. Chem., Int. Ed.* **2020**, *59*, 596–612.
- (4) Miras, H. N.; Cooper, G. J. T.; Long, D.-L.; Bögge, H.; Müller, A.; Streb, C.; Cronin, L. Unveiling the Transient Template in the Self-Assembly of a Molecular Oxide Nanowheel. *Science* **2010**, *327*, 72–74.
- (5) Müller, A.; Das, S. K.; Bögge, H.; Beugholt, C.; Schmidtmann, M. Assembling Nanosized Ring-Shaped Synthons to an Anionic Layer Structure Based on the Synergetically Induced Functional Complementarity of Their Surface-Sites: $\text{Na}_2\text{[MoV126MoV28O462H14(H}_2\text{O)}_{54}(\text{H}_2\text{PO}_4)_7]\text{xH}_2\text{O}$ ($\text{x} \approx 300$). *Chem. Commun.* **1999**, 1035–1036.
- (6) Xuan, W.; Surman, A. J.; Miras, H. N.; Long, D.-L.; Cronin, L. Controlling the Ring Curvature, Solution Assembly, and Reactivity of Gigantic Molybdenum Blue Wheels. *J. Am. Chem. Soc.* **2014**, *136*, 14114–14120.

- (7) Müller, A.; Beugholt, C.; Bögge, H.; Schmidtmann, M. Influencing the Size of Giant Rings by Manipulating Their Curvatures: $\text{Na}_6[\text{Mo}_{12}\text{O}_{36}(\text{H}_2\text{O})_{48}\text{H}_{12}\{\text{Pr}(\text{H}_2\text{O})_5\}_6] \cdot (\sim 200\text{H}_2\text{O})$ with Open Shell Metal Centers at the Cluster Surface. *Inorg. Chem.* **2000**, *39*, 3112–3113.
- (8) Müller, A.; Beckmann, E.; Bögge, H.; Schmidtmann, M.; Dress, A. Inorganic Chemistry Goes Protein Size: A Mo_{36} Nano-Hedgehog Initiating Nanochemistry by Symmetry Breaking. *Angew. Chem., Int. Ed.* **2002**, *41*, 1162–1167.
- (9) Li, H.; Yang, W.; Chai, Y.; Chen, L.; Zhao, J. A Novel Dawson-like Cerium(IV)-Hybridizing Selenotungstate $\text{Na}_{13}\text{H}_7[\text{Ce}(\text{SeW17OS9})_2] \cdot 31\text{H}_2\text{O}$. *Inorg. Chem. Commun.* **2015**, *56*, 35–40.
- (10) Hu, H.; Pang, J.; Gong, P.; Chen, L.; Zhao, J. Organic-Inorganic Two-Dimensional Hybrid Networks Constructed from Pyridine-4-Carboxylate-Decorated Organotin–Lanthanide Heterometallic Antimotungstates. *Inorg. Chem.* **2020**, *59*, 11287–11297.
- (11) Wang, D.; Li, Y.; Zhang, Y.; Xu, X.; Liu, Y.; Chen, L.; Zhao, J. Construction of Ln_3+ -Substituted Arsenotungstates Modified by 2,5-Thiophenedicarboxylic Acid and Application in Selective Fluorescence Detection of Ba^{2+} in Aqueous Solution. *Inorg. Chem.* **2020**, *59*, 6839–6848.
- (12) Fernandes, D. M.; Cunha-Silva, L.; Ferreira, R. A. S.; Balula, S. S.; Carlos, L. D.; de Castro, B.; Freire, C. Redox Behaviour, Electrochromic Properties and Photoluminescence of Potassium Lanthano Phosphomolybdate Sandwich-Type Compounds. *RSC Adv.* **2013**, *3*, 16697–16707.
- (13) Molina, P. I.; Sures, D. J.; Miró, P.; Zakharov, L. N.; Nyman, M. Bridging the Opposite Chemistries of Tantalum and Tungsten Polyoxometalates. *Dalton Trans.* **2015**, *44*, 15813–15822.
- (14) Deblonde, G. J.-P.; Chagnes, A.; Cote, G.; Vial, J.; Rivals, I.; Delaunay, N. Development of a Capillary Electrophoresis Method for the Analysis in Alkaline Media as Polyoxoanions of Two Strategic Metals: Niobium and Tantalum. *J. Chromatogr. A* **2016**, *1437*, 210–218.
- (15) De Cock, B.; Oliver, J. D.; Delaunay, N.; Deblonde, G.; Mangelings, D.; Heyden, Y. V. Interinstrumental Transfer of a Fast Short-End Injection Capillary Electrophoresis Method: Application to the Separation of Niobium, Tantalum, and Their Substituted Ions. *Electrophoresis* **2017**, *38*, 2069–2074.
- (16) Zhang, D.; Zhang, C.; Ma, P.; Bassil, B. S.; Al-Oweini, R.; Kortz, U.; Wang, J.; Niu, J. Two New Members of the Niobium-Substituted Polytungstophosphate Family Based on Hexalacunary $[\text{H}_2\text{P}_2\text{W}_{12}\text{O}_{48}]^{12-}$ Building Blocks. *Inorg. Chem. Front.* **2015**, *2*, 254–262.
- (17) Ma, X.; Li, H.; Chen, L.; Zhao, J. The Main Progress over the Past Decade and Future Outlook on High-Nuclear Transition-Metal Substituted Polyoxotungstates: From Synthetic Strategies, Structural Features to Functional Properties. *Dalton Trans.* **2016**, *45*, 4935–4960.
- (18) Das, V.; Kaushik, R.; Hussain, F. Heterometallic 3d-4f Polyoxometalates: An Emerging Field with Structural Diversity to Multiple Applications. *Coord. Chem. Rev.* **2020**, *413*, No. 213271.
- (19) Blasco-Ahicart, M.; Soriano-López, J.; Carbó, J. J.; Poblet, J. M.; Galan-Mascaro, J. R. Polyoxometalate Electrocatalysts Based on Earth-Abundant Metals for Efficient Water Oxidation in Acidic Media. *Nat. Chem.* **2018**, *10*, 24–30.
- (20) Neumann, R.; Dahan, M. A Ruthenium-Substituted Polyoxometalate as an Inorganic Dioxygenase for Activation of Molecular Oxygen. *Nature* **1997**, *388*, 353–355.
- (21) Maksimchuk, N. V.; Evtushok, V. Yu.; Zalomaeva, O. V.; Maksimov, G. M.; Ivanchikova, I. D.; Chesalov, Y. A.; Eltsov, I. V.; Abramov, P. A.; Glazneva, T. S.; Yanshole, V. V.; Kholdeeva, O. A.; Errington, R. J.; Solé-Daura, A.; Poblet, J. M.; Carbó, J. J. Activation of H_2O_2 over $\text{Zr}(\text{IV})$. Insights from Model Studies on Zr-Monosubstituted Lindqvist Tungstates. *ACS Catal.* **2021**, *11*, 10589–10603.
- (22) Chen, J.-J.; Symes, M. D.; Cronin, L. Highly Reduced and Protonated Aqueous Solutions of $[\text{P}_2\text{W}_{18}\text{O}_{62}]^{6-}$ for on-Demand Hydrogen Generation and Energy Storage. *Nat. Chem.* **2018**, *10*, 1042–1047.
- (23) Gao, N.; Sun, H.; Dong, K.; Ren, J.; Duan, T.; Xu, C.; Qu, X. Transition-Metal-Substituted Polyoxometalate Derivatives as Functional Anti-Amyloid Agents for Alzheimer's Disease. *Nat. Commun.* **2014**, *5*, No. 3422.
- (24) Judd, D. A.; Nettles, J. H.; Nevins, N.; Snyder, J. P.; Liotta, D. C.; Tang, J.; Ermolieff, J.; Schinazi, R. F.; Hill, C. L. Polyoxometalate HIV-1 Protease Inhibitors. A New Mode of Protease Inhibition. *J. Am. Chem. Soc.* **2001**, *123*, 886–897.
- (25) Katsoulis, D. E. A Survey of Applications of Polyoxometalates. *Chem. Rev.* **1998**, *98*, 359–388.
- (26) Dong, J.; Lv, H.; Sun, X.; Wang, Y.; Ni, Y.; Zou, B.; Zhang, N.; Yin, A.; Chi, Y.; Hu, C. A Versatile Self-Detoxifying Material Based on Immobilized Polyoxoniobate for Decontamination of Chemical Warfare Agent Simulants. *Chem. – Eur. J.* **2018**, *24*, 19208–19215.
- (27) Kinnan, M. K.; Creasy, W. R.; Fullmer, L. B.; Schreuder-Gibson, H. L.; Nyman, M. Nerve Agent Degradation with Polyoxoniobates. *Eur. J. Inorg. Chem.* **2014**, *2014*, 2361–2367.
- (28) Busche, C.; Vilà-Nadal, L.; Yan, J.; Miras, H. N.; Long, D.-L.; Georgiev, V. P.; Asenov, A.; Pedersen, R. H.; Gadegaard, N.; Mirza, M. M.; Paul, D. J.; Poblet, J. M.; Cronin, L. Design and Fabrication of Memory Devices Based on Nanoscale Polyoxometalate Clusters. *Nature* **2014**, *515*, 545–549.
- (29) Gaita-Ariño, A.; Luis, F.; Hill, S.; Coronado, E. Molecular Spins for Quantum Computation. *Nat. Chem.* **2019**, *11*, 301–309.
- (30) Jin, Z.; Bai, J.; Wei, T.; Li, F.; Song, C.; Luo, X.; Xu, L. A New Series of Mononuclear Lanthanide Single Molecule Magnets Based on Sandwich-Type Germanomolybdates $[\text{Ln}(\text{GeMo}_{11}\text{O}_{39})_2]^{13-}$ ($\text{Ln} = \text{Er}^{\text{III}}$, Gd^{III} , Dy^{III} or Tb^{III}). *New J. Chem.* **2017**, *41*, 13490–13494.
- (31) Rustad, J. R.; Casey, W. H. Metastable Structures and Isotope Exchange Reactions in Polyoxometalate Ions Provide a Molecular View of Oxide Dissolution. *Nat. Mater.* **2012**, *11*, 223–226.
- (32) Yang, D.; Babucci, M.; Casey, W. H.; Gates, B. C. The Surface Chemistry of Metal Oxide Clusters: From Metal–Organic Frameworks to Minerals. *ACS Cent. Sci.* **2020**, *6*, 1523–1533.
- (33) Peacock, R. D.; Weakley, T. J. R. Heteropolytungstate Complexes of the Lanthanide Elements. Part I. Preparation and Reactions. *J. Chem. Soc. A* **1971**, 1836–1839.
- (34) Iijima, J.; Naruke, H.; Sanji, T. Chirality Induction in Crystalline Solids Containing Sandwich-Type $[\text{Ln}(\text{A}_2\text{P}_2\text{W}_{17}\text{O}_{61})_2]^{17-}$ Polyoxotungstates and Proline. *Inorg. Chem.* **2018**, *57*, 13351–13363.
- (35) Zhang, C.; Howell, R. C.; Scotland, K. B.; Perez, F. G.; Todaro, L.; Francesconi, L. C. Aqueous Speciation Studies of Europium(III) Phosphotungstate. *Inorg. Chem.* **2004**, *43*, 7691–7701.
- (36) Auvergne, T.; Matson, E. M. Polyoxometalate-Based Complexes as Ligands for the Study of Actinide Chemistry. *Dalton Trans.* **2020**, *49*, 13917–13927.
- (37) Copper, R.; Talbot-Eeckelaers, C.; Collison, D.; Helliwell, M.; Gaunt, A. J.; May, I.; Reilly, S. D.; Scott, B. L.; McDonald, R. D.; Valenzuela, O. A.; Jones, C. J.; Sarsfield, M. J. Probing the Sf Electrons in a Plutonyl(VI) Cluster Complex. *Dalton Trans.* **2009**, *5609–5611*.
- (38) Sokolova, M. N.; Fedossev, A. M.; Andreev, G. B.; Budantseva, N. A.; Yusov, A. B.; Moisy, P. Synthesis and Structural Examination of Complexes of $\text{Am}(\text{IV})$ and Other Tetravalent Actinides with Lacunary Heteropolyanion $\text{A}_2\text{P}_2\text{W}_{17}\text{O}_{6110}^-$. *Inorg. Chem.* **2009**, *48*, 9185–9190.
- (39) Colliard, I.; Lee, J. R. I.; Colla, C. A.; Mason, H. E.; Sawvel, A. M.; Zavarin, M.; Nyman, M.; Deblonde, G. J.-P. Polyoxometalates as Ligands to Synthesize, Isolate and Characterize Compounds of Rare Isotopes on the Microgram Scale. *Nat. Chem.* **2022**, *14*, 1357–1366.
- (40) Antonio, M. R.; Williams, C. W.; Soderholm, L. Synthesis and Characterization of Actinide-Exchanged Preyssler Heteropolyanions $[\text{AnPSW}_{30}\text{O}_{110}]^{N-}$ ($\text{An} \equiv \text{Th}$, Am , Cm). *J. Alloys Compd.* **1998**, *271–273*, 846–849.
- (41) Chiang, M.-H.; Soderholm, L.; Antonio, M. R. Redox Chemistry of Actinide Ions in Wells–Dawson Heteropolyoxoanion Complexes. *Eur. J. Inorg. Chem.* **2003**, *2003*, 2929–2936.
- (42) Ioussou, A.; Krupa, J. C. Luminescence Properties and Stability Constants of Curium(III) Complexes with Lacunary Heteropolyan-

- ions PW11O397- and SiW11O398- in Nitric Acid Solutions. *Radiochim. Acta* **1997**, *78*, 97–104.
- (43) Milyukova, M. S.; Malikov, D. A.; Kuzovkina, E. V.; Myasoedov, B. F. Extraction of Tetravalent Berkelium by High Molecular Weight Amines in the Presence of Heteropolyanions. *J. Radioanal. Nucl. Chem. Lett.* **1986**, *104*, 81–89.
- (44) Choppin, G. R.; Wall, D. E. Interaction of Actinide Ions with [NaPSW3O110]14- and [P2W18O62]6-. *J. Radioanal. Nucl. Chem.* **2003**, *255*, 47–52.
- (45) Antonio, M. R.; Chiang, M.-H. Stabilization of Plutonium(III) in the Preyssler Polyoxometalate. *Inorg. Chem.* **2008**, *47*, 8278–8285.
- (46) Baranov, M.; Tubul, T.; Azulai, Y.; Weinstock, I. A. A Simple Coulombic Model for ^{31}P NMR Spectra of Cluster-Encapsulated Phosphorus Atoms. *Inorg. Chem.* **2019**, *58*, 8877–8883.
- (47) Panasci, A. F.; Harley, S. J.; Zavarin, M.; Casey, W. H. Kinetic Studies of the [NpO₂(CO₃)₃]4- Ion at Alkaline Conditions Using ^{13}C NMR. *Inorg. Chem.* **2014**, *53*, 4202–4208.
- (48) Balogh, E.; Anderson, T. M.; Rustad, J. R.; Nyman, M.; Casey, W. H. Rates of Oxygen-Isotope Exchange between Sites in the [HxTa₆O₁₉](8-x)-(Aq) Lindqvist Ion and Aqueous Solutions: Comparisons to [HxNb₆O₁₉](8-x)-(Aq). *Inorg. Chem.* **2007**, *46*, 7032–7039.
- (49) Villa, E. M.; Ohlin, C. A.; Casey, W. H. Oxygen-Isotope Exchange Rates for Three Isostructural Polyoxometalate Ions. *J. Am. Chem. Soc.* **2010**, *132*, 5264–5272.
- (50) Villa, E. M.; Ohlin, C. A.; Rustad, J. R.; Casey, W. H. Isotope-Exchange Dynamics in Isostructural Decametalates with Profound Differences in Reactivity. *J. Am. Chem. Soc.* **2009**, *131*, 16488–16492.
- (51) Ochoa, G.; Pilgrim, C. D.; Martin, M. N.; Colla, C. A.; Klavins, P.; Augustine, M. P.; Casey, W. H. ^{2}H and ^{139}La NMR Spectroscopy in Aqueous Solutions at Geochemical Pressures. *Angew. Chem.* **2015**, *127*, 15664–15667.
- (52) Oliveri, A. F.; Colla, C. A.; Perkins, C. K.; Akhavantabib, N.; Callahan, J. R.; Pilgrim, C. D.; Smart, S. E.; Cheong, P. H.-Y.; Pan, L.; Casey, W. H. Isomerization of Keggin Al₁₃ Ions Followed by Diffusion Rates. *Chem. – Eur. J.* **2016**, *22*, 18637–18637.
- (53) Roberto, J. B.; Rykaczewski, K. P. Discovery of Element 117: Super-Heavy Elements and the “Island of Stability”*. *Sep. Sci. Technol.* **2018**, *53*, 1813–1819.
- (54) Deblonde, G. J.-P.; Mattocks, J. A.; Dong, Z.; Woody, P. T.; Cotruvo, J. A.; Zavarin, M. Capturing an Elusive but Critical Element: Natural Protein Enables Actinium Chemistry. *Sci. Adv.* **2021**, *7*, No. eabk0273.
- (55) Stein, B. W.; Morgenstern, A.; Batista, E. R.; Birnbaum, E. R.; Bone, S. E.; Cary, S. K.; Ferrier, M. G.; John, K. D.; Pacheco, J. L.; Kozimor, S. A.; Mocko, V.; Scott, B. L.; Yang, P. Advancing Chelation Chemistry for Actinium and Other +3 F-Elements, Am, Cm, and La. *J. Am. Chem. Soc.* **2019**, *141*, 19404–19414.
- (56) Goodwin, C. A. P.; Su, J.; Albrecht-Schmitt, T. E.; Blake, A. V.; Batista, E. R.; Daly, S. R.; Dehnen, S.; Evans, W. J.; Gaunt, A. J.; Kozimor, S. A.; Lichtenberger, N.; Scott, B. L.; Yang, P. [Am-(CSMe₄H₃)]: An Organometallic Americium Complex. *Angew. Chem., Int. Ed.* **2019**, *58*, 11695–11699.
- (57) Windorff, C. J.; Celis-Barros, C.; Sperling, J. M.; McKinnon, N. C.; Albrecht-Schmitt, T. E. Probing a Variation of the Inverse-Trans-Influence in Americium and Lanthanide Tribromide Tris-(Tricyclohexylphosphine Oxide) Complexes. *Chem. Sci.* **2020**, *11*, 2770–2782.
- (58) Greer, R. D. M.; Celis-Barros, C.; Sperling, J. M.; Gaiser, A. N.; Windorff, C. J.; Albrecht-Schönzart, T. E. Structure and Characterization of an Americium Bis(O,O'-Diethyl)Dithiophosphate Complex. *Inorg. Chem.* **2020**, *59*, 16291–16300.
- (59) Sittel, T.; Weßling, P.; Großmann, D.; Engels, E.; Geist, A.; Panak, P. J. Spectroscopic Investigation of the Covalence of An(III) Complexes with Tetraethylcarboxamidopyridine. *Dalton Trans.* **2022**, *51*, 8028–8035.
- (60) Goodwin, C. A. P.; Su, J.; Stevens, L. M.; White, F. D.; Anderson, N. H.; Auxier, J. D.; Albrecht-Schönzart, T. E.; Batista, E. R.; Briscoe, S. F.; Cross, J. N.; Evans, W. J.; Gaiser, A. N.; Gaunt, A. J.; James, M. R.; Janicke, M. T.; Jenkins, T. F.; Jones, Z. R.; Kozimor, S. A.; Scott, B. L.; Sperling, J. M.; Wedal, J. C.; Windorff, C. J.; Yang, P.; Ziller, J. W. Isolation and Characterization of a Californium Metallocene. *Nature* **2021**, *599*, 421–424.
- (61) Adam, C.; Beele, B. B.; Geist, A.; Müllrich, U.; Kaden, P.; Panak, P. J. NMR and TRLFS Studies of Ln(III) and An(III) C₅-BPP Complexes. *Chem. Sci.* **2015**, *6*, 1548–1561.
- (62) Adam, C.; Kaden, P.; Beele, B. B.; Müllrich, U.; Trumm, S.; Geist, A.; Panak, P. J.; Denecke, M. A. Evidence for Covalence in a N-Donor Complex of Americium(III). *Dalton Trans.* **2013**, *42*, 14068–14074.
- (63) Wall, T. F.; Jan, S.; Autillo, M.; Nash, K. L.; Guerin, L.; Naour, C. L.; Moisy, P.; Berthon, C. Paramagnetism of Aqueous Actinide Cations. Part I: Perchloric Acid Media. *Inorg. Chem.* **2014**, *53*, 2450–2459.
- (64) Autillo, M.; Kaden, P.; Geist, A.; Guerin, L.; Moisy, P.; Berthon, C. The Influence of Radioactive Decay on Actinide Magnetic Susceptibility Measurements Obtained Using the Evans Method. *Phys. Chem. Chem. Phys.* **2014**, *16*, 8608–8614.
- (65) Autillo, M.; Guerin, L.; Bolvin, H.; Moisy, P.; Berthon, C. Magnetic Susceptibility of Actinide(III) Cations: An Experimental and Theoretical Study. *Phys. Chem. Chem. Phys.* **2016**, *18*, 6515–6525.
- (66) Autillo, M.; Guerin, L.; Dumas, T.; Grigoriev, M. S.; Fedoseev, A. M.; Cammelli, S.; Solari, P. L.; Guillaumont, D.; Guilbaud, P.; Moisy, P.; Bolvin, H.; Berthon, C. Insight of the Metal–Ligand Interaction in f-Element Complexes by Paramagnetic NMR Spectroscopy. *Chem. – Eur. J.* **2019**, *25*, 4435–4451.
- (67) Contant, R.; Klemperer, W. G.; Yaghi, O. Potassium Octadecatungstodiphosphates(V) and Related Lacunary Compounds. In *Inorganic Syntheses*; John Wiley & Sons, Ltd, 1990; pp 104–111.
- (68) Tézé, A.; Cadot, E.; Béreau, V.; Hervé, G. About the Keggin Isomers: Crystal Structure of [N(C₄H₉)₄]4-γ-[SiW₁₂O₄₀], the γ-Isomer of the Keggin Ion. Synthesis and ^{183}W NMR Characterization of the Mixed γ-[SiMo₂W₁₀O₄₀]_n-(n = 4 or 6). *Inorg. Chem.* **2001**, *40*, 2000–2004.
- (69) Wang, S.-H.; Jansen, S. A. The “Alternate” Keggin Ion: A Theoretical Study of the Stability Factors for the Beta-Keggin Ion in Comparison with the Corresponding Alpha-Keggin Ion. *Chem. Mater.* **1994**, *6*, 2130–2137.
- (70) Weinstock, I. A.; Cowan, J. J.; Barbuzzi, E. M. G.; Zeng, H.; Hill, C. L. Equilibria between α and β Isomers of Keggin Heteropolytungstates. *J. Am. Chem. Soc.* **1999**, *121*, 4608–4617.
- (71) Lundberg, D.; Persson, I. The Size of Actinoid(III) Ions – Structural Analysis vs. Common Misinterpretations. *Coord. Chem. Rev.* **2016**, *318*, 131–134.
- (72) Firsching, F. H.; Brune, S. N. Solubility Products of the Trivalent Rare-Earth Phosphates. *J. Chem. Eng. Data* **1991**, *36*, 93–95.
- (73) Parker, D.; Suturina, E. A.; Kuprov, I.; Chilton, N. F. How the Ligand Field in Lanthanide Coordination Complexes Determines Magnetic Susceptibility Anisotropy, Paramagnetic NMR Shift, and Relaxation Behavior. *Acc. Chem. Res.* **2020**, *53*, 1520–1534.
- (74) Li, N.; García-Rodríguez, R.; Matthews, P. D.; Luo, H.-K.; Wright, D. S. Synthesis, Structure and Paramagnetic NMR Analysis of a Series of Lanthanide-Containing [LnTi₆O₃(O₂Pr)₉(Salicylate)₆] Cages. *Dalton Trans.* **2017**, *46*, 4287–4295.
- (75) Horne, G. P.; Mezyk, S. P.; Mincher, B. J.; Zarzana, C. A.; Rae, C.; Tillotson, R. D.; Schmitt, N. C.; Ball, R. D.; Ceder, J.; Charbonnel, M.-C.; Guilbaud, P.; Saint-Louis, G.; Berthon, L. DEHBA (Di-2-Ethylhexylbutyramide) Gamma Radiolysis under Spent Nuclear Fuel Solvent Extraction Process Conditions. *Radiat. Phys. Chem.* **2020**, *170*, No. 108608.
- (76) Barros, C. C.; Pilgrim, C. D.; Cook, A. R.; Mezyk, S. P.; Grimes, T. S.; Horne, G. P. Influence of Uranyl Complexation on the Reaction Kinetics of the Dodecane Radical Cation with Used Nuclear Fuel Extraction Ligands (TBP, DEHBA, and DEHiBA). *Phys. Chem. Chem. Phys.* **2021**, *23*, 24589–24597.
- (77) Kimberlin, A.; Saint-Louis, G.; Guillaumont, D.; Camès, B.; Guilbaud, P.; Berthon, L. Effect of Metal Complexation on

Diglycolamides Radiolysis: A Comparison between Ex-Situ Gamma and In-Situ Alpha Irradiation. *Phys. Chem. Chem. Phys.* **2022**, DOI: 10.1039/D1CP05731F.

(78) Evans, D. F. 400. The Determination of the Paramagnetic Susceptibility of Substances in Solution by Nuclear Magnetic Resonance. *J. Chem. Soc.* **1959**, 2003–2005.

(79) Cary, S. K.; Vasiliu, M.; Baumbach, R. E.; Stritzinger, J. T.; Green, T. D.; Diefenbach, K.; Cross, J. N.; Knappenberger, K. L.; Liu, G.; Silver, M. A.; DePrince, A. E.; Polinski, M. J.; Cleve, S. M. V.; House, J. H.; Kikugawa, N.; Gallagher, A.; Arico, A. A.; Dixon, D. A.; Albrecht-Schmitt, T. E. Emergence of Californium as the Second Transitional Element in the Actinide Series. *Nat. Commun.* **2015**, *6*, No. 6827.

(80) Silver, M. A.; Cary, S. K.; Johnson, J. A.; Baumbach, R. E.; Arico, A. A.; Luckey, M.; Urban, M.; Wang, J. C.; Polinski, M. J.; Chemey, A.; Liu, G.; Chen, K.-W.; Cleve, S. M. V.; Marsh, M. L.; Eaton, T. M.; van de Burgt, L. J.; Gray, A. L.; Hobart, D. E.; Hanson, K.; Maron, L.; Gendron, F.; Autschbach, J.; Speldrich, M.; Kögerler, P.; Yang, P.; Braley, J.; Albrecht-Schmitt, T. E. Characterization of Berkelium(III) Dipicolinate and Borate Compounds in Solution and the Solid State. *Science* **2016**, *353*, No. aaf3762.

(81) Albrecht-Schmitt, T. E.; Hobart, D. E.; Páez-Hernández, D.; Celis-Barros, C. Theoretical Examination of Covalency in Berkelium-(IV) Carbonate Complexes. *Int. J. Quantum Chem.* **2020**, *120*, No. e26254.

(82) Moll, H.; Brendler, V.; Bernhard, G. Aqueous Curium(III) Phosphate Species Characterized by Time-Resolved Laser-Induced Fluorescence Spectroscopy. *Radiochim. Acta* **2011**, *99*, 775–782.

(83) Huittinen, N.; Jessat, I.; Réal, F.; Vallet, V.; Starke, S.; Eibl, M.; Jordan, N. Revisiting the Complexation of Cm(III) with Aqueous Phosphates: What Can We Learn from the Complex Structures Using Luminescence Spectroscopy and Ab Initio Simulations? *Inorg. Chem.* **2021**, *60*, 10656–10673.

(84) Lundberg, D.; Persson, I.; Eriksson, L.; D'Angelo, P.; De Panfilis, S. Structural Study of the N,N'-Dimethylpropyleneurea Solvated Lanthanoid(III) Ions in Solution and Solid State with an Analysis of the Ionic Radii of Lanthanoid(III) Ions. *Inorg. Chem.* **2010**, *49*, 4420–4432.

(85) Oliveri, A. F.; Carnes, M. E.; Baseman, M. M.; Richman, E. K.; Hutchison, J. E.; Johnson, D. W. Single Nanoscale Cluster Species Revealed by ¹H NMR Diffusion-Ordered Spectroscopy and Small-Angle X-Ray Scattering. *Angew. Chem., Int. Ed.* **2012**, *51*, 10992–10996.

CAS BIOFINDER DISCOVERY PLATFORM™

ELIMINATE DATA SILOS. FIND WHAT YOU NEED, WHEN YOU NEED IT.

A single platform for relevant, high-quality biological and toxicology research

Streamline your R&D

CAS 
A division of the
American Chemical Society